

UCSD/PTH 97-20

# Explicit Quark-hadron Duality in Heavy-light Meson Weak Decays in the 't Hooft Model

Benjamn Grinstein\* and Richard F. Lebed†

*Department of Physics, University of California at San Diego, La Jolla, CA 92093*

(August 18, 1997)

## Abstract

We compute the nonleptonic weak decay width of a heavy-light meson in 1+1 spacetime dimensions with a large number of QCD colors (the 't Hooft model) as a function of the heavy quark mass. In this limit, QCD is exactly soluble, and decay modes are dominated by two-particle final states. We compare the results to the tree-level partonic decay width of the heavy quark in order to test quark-hadron duality in this universe. We find that this duality is surprisingly well satisfied in the heavy quark limit, in that the difference between the sum of exclusive partial widths and the tree-level partonic width approaches a constant as  $M \rightarrow \infty$ , and the deviation is well-fit by a small  $1/M$  correction. We comment on the meaning of this conclusion and its implications for the use of quark-hadron duality in hadronic physics.

11.10.Kk, 11.15.Pg, 13.25-k

Typeset using REVTeX

---

\*bgrinstein@ucsd.edu

†rlebed@ucsd.edu

## I. INTRODUCTION

Quark-hadron duality, in its most general form, is the notion that certain rates for processes involving hadrons can be computed simply as the underlying partonic rates [1]. Duality allows us to compute many quantities which would otherwise be hopelessly difficult. One common application of duality is to the nonleptonic weak decays of heavy hadrons. The lore is that, for large enough heavy quark mass, duality holds in the computation of the hadronic width.

Several discrepancies between theory and experiment that have recently received attention rely on quark-hadron duality. Among them are the significant difference between lifetimes of beauty baryons and mesons [2], the overestimates of the  $B$ -meson semileptonic branching fraction [3] and the average number of charm quarks per  $B$  decay [4]. Because the limit of experimental knowledge about nonleptonic  $B$  decays is rapidly expanding, such issues are of great topical interest.

But when is duality valid? In many cases duality follows from the Operator Product Expansion (OPE). This is the case, for example, for the rate of  $e^+e^- \rightarrow$  hadrons and for the semileptonic decay rates of heavy hadrons. However, duality is applied in many other cases, such as in hadronic widths of heavy hadrons, for which there is no OPE.

Reference [5] proposes an OPE-like expansion in inverse powers of the heavy quark mass  $M$ , which not only incorporates quark-hadron duality as the lowest term in the expansion, but also organizes the corrections by inverse powers of  $M$ . A main result of that work is the claim that corrections first appear at order  $1/M^2$ . The question above can be reformulated as, “Is an OPE-like expansion like that of Ref. [5] valid?”

To investigate the validity of duality it is convenient to work with a soluble model of strong interactions formulated as a full-fledged field theory, so that one may test duality both in cases with and without an OPE. The 't Hooft model [6], large- $N_c$  QCD in 1+1 dimensions, is a good laboratory for this purpose. It contains an infinite spectrum of mesons composed of confined quarks, realizes asymptotic freedom trivially, and inherits all the phenomenological consequences of large- $N_c$  QCD [7] common to our universe, such as dominance of scattering amplitudes with the minimum number of meson states, OZI suppression, the absence of exotics, and others. For processes with an OPE, duality in the 't Hooft model has been checked explicitly [8,9]. However, little is known about duality for non-OPE processes. The reason is that, in precisely those cases for which an OPE is lacking, there is no simple analytical method of verifying duality, and one must resort to arguments based on numerical solutions.

In this paper we compute the hadronic weak decay width  $\Gamma(M)$  of heavy “ $B$ ” mesons in the 't Hooft model as a function of the heavy “ $b$ ” quark mass  $M$ ; the meaning of “heavy” is made precise in Sec. II. We compare this to the partonic (perturbative) decay width of the heavy quark,  $\Gamma_{\text{part}}(M)$ , which we compute analytically. For large  $M$  we find that both  $\Gamma_{\text{part}}(M)$  and  $\Gamma(M)$  are essentially linear in  $M$ . The difference between the two appears to be asymptotically constant and small, indicating a small  $1/M$  correction to the naive duality limit. As  $M$  increases, new hadronic decay channels become accessible, and at each of these thresholds there is a singular peak in  $\Gamma(M)$ . Averaging  $\Gamma(M)$  over a region in  $M$  that includes many resonances removes these peaks but does not change the leading dependence on  $M$ . *Our conclusion is that duality holds to leading order in  $M$ , but unlike the OPE-like*

expansion of Ref. [5], appears to have  $1/M$  corrections.

In Ref. [10] it is argued that there is strong experimental evidence for the failure of duality. What is meant there is that the pattern of corrections in powers of  $1/M$  of Ref. [5] is not supported by experiment. This agrees with our result, which indicates a violation to duality at first order in the  $1/M$  expansion of Ref. [5].

While we cannot carry over our quantitative results to the physical world of non-planar QCD in  $3+1$  dimensions, we believe that there is nothing intrinsic to  $1+1$  dimensions that would make duality work differently than in  $3+1$ . The operator analysis that leads to the  $1/M$  expansion proceeds in  $1+1$  much as in  $3+1$ .

The paper is organized as follows. In Sec. II, we briefly review the 't Hooft model and a standard method for its numerical solution. Section III compares features of  $1+1$  dimensions, such as the nature of phase space and spin, to those in  $3+1$  dimensions. In Sec. IV, we present the algebraic results of the inclusive parton-level calculation of widths. In Sec. V, we present the results of the exclusive calculation in the 't Hooft model. Section VI gives our numerical results and a discussion of their implications, and Sec. VII concludes.

There are other nonperturbative questions of phenomenological interest in the area of hadronic  $B$  weak decays for which there is an established lore. One can test any of these hypotheses in the 't Hooft model. Of particular interest is the notion that contributions to decay amplitudes from different underlying quark diagram topologies contribute with distinct weights, which can very much suppress the amplitude from a given topology. For example, the “annihilation” diagrams, in which the valence quark-antiquark pair annihilate through a weak current, are supposedly suppressed relative the “spectator” diagrams by a factor of  $f_B/M_B$ , where  $f_B$  is the  $B$  decay constant and  $M_B$  its mass. We will address this question in a separate publication [11].

## II. THE 'T HOOFT MODEL

The success of 't Hooft's method of solving a strongly-coupled theory rests on two assumptions that considerably simplify the problem. First, one works in the limit of large  $N_c$ , in which it is readily seen [7] that diagrams including either internal fermion-antifermion loops or the crossing of gluon lines at points other than their vertices are suppressed by combinatorial powers of  $N_c$  compared to those that do not. These simple topological consequences of the theory lead directly to the predictive power of large  $N_c$ . Second, in  $1+1$  dimensions one may use the gauge freedom of QCD to choose a linear gauge in which some chosen component of the gluon field vanishes, and only the sole orthogonal component survives. Then, since the gluon self-coupling term in the field strength appears as a commutator of field components, this term vanishes in the gauge we have selected. Consequently, gluon self-coupling vanishes in this gauge, and so in combination with large  $N_c$ , gluon lines are not permitted to cross each other, even at vertices. Moreover, ghosts are absent in linear gauges. It follows that the only diagrams that must be summed are “rainbow” diagrams for the quark mass and wave function renormalization, and “ladder” diagrams for quark-antiquark interactions [6].

In  $1+1$  dimensions confinement is realized trivially, since the lowest-order inter-quark potential obtained by taking the Fourier transform of the gluon propagator (which gives rise to the  $1/r$  Coulomb interaction in four dimensions) grows linearly with the inter-quark

separation. Although lowest-order color confinement is an automatic consequence in two dimensions, it is a highly nontrivial fact that the phenomenon persists in the all-orders Green function solutions of the 't Hooft model.

To be specific, the Lagrangian of QCD, as in four dimensions, is

$$\mathcal{L} = -\frac{1}{4} \text{Tr} F_{\mu\nu} F^{\mu\nu} + \sum_a \bar{\psi}_a (\gamma^\mu (i\partial_\mu - gA_\mu) - m_a) \psi_a, \quad (2.1)$$

where  $A_\mu$  is the  $SU(N_c)$  gauge field with field strength  $F_{\mu\nu}$  defined in the usual way, and  $\psi_a$  is a Dirac fermion of bare mass  $m_a$  and flavor  $a$ . The bare coupling  $g$  not only has dimensions of mass in two dimensions, but scales as  $1/\sqrt{N_c}$  in the large- $N_c$  limit.

The renormalization of the fermion propagator is exceptionally simple. The only modification is a shift of the bare fermion mass by

$$m_a^2 \rightarrow m_{a,R}^2 \equiv m_a^2 - g^2 N_c / 2\pi. \quad (2.2)$$

Consequently, it makes good sense to describe masses in units of  $g\sqrt{N_c/2\pi}$ , which is finite in the  $N_c \rightarrow \infty$  limit. The dividing line of  $m_a^2 = 1$  ( $m_{a,R}^2 = 0$ ) in these units acts as a boundary between heavy and light quarks, as is numerically verified in Refs. [12–14]; for example, in [13] it was seen that the meson decay constant approaches the standard asymptotic behavior  $f_B \propto 1/\sqrt{M}$  for  $M \geq 5$  or so. It follows that  $g\sqrt{N_c/2\pi}$  in 1+1 assumes a role analogous to  $\Lambda_{\text{QCD}}$  in 3+1.

Quantization of the theory is most convenient in axial light-cone gauge ( $A_- = 0$ ), where light cone coordinates are defined by

$$x^\pm \equiv x_\mp \equiv \frac{(x^0 \pm x^1)}{\sqrt{2}}, \quad (2.3)$$

and analogously for other vectors. The chief advantage of this choice is that only one component of the Dirac algebra ( $\gamma_-$ ) survives, thus effectively eliminating the need to perform Dirac traces.

Upon solving for the Green function of a fermion-antifermion pair with bare masses  $M$  and  $m$  in this model, one obtains the bound-state eigenvalue equation

$$\mu_n^2 \phi_n^{M\overline{m}}(x) = \left( \frac{M_R^2}{x} + \frac{m_R^2}{1-x} \right) \phi_n^{M\overline{m}}(x) - \int_0^1 dy \phi_n^{M\overline{m}}(y) \text{Pr} \frac{1}{(y-x)^2}, \quad (2.4)$$

which is known as the 't Hooft equation [6]. Here the  $n$ th eigenstate  $\phi_n^{M\overline{m}}$  is the meson wave function, the  $n$ th eigenvalue  $\mu_n^2$  is its squared mass, and  $x$  is the fraction of the meson momentum's minus component (which acts, in the light-cone quantization, as a canonical spatial momentum component) carried by quark  $M$ . We will always label the ground state (the lowest mass meson) by  $n = 0$ . The principal value prescription serves to regulate the integrand singularity, which originates in the infrared divergence of the gluon propagator. This equation has a discrete spectrum of eigenvalues that increase approximately linearly for large  $n$ , and the wave functions vanish at the boundaries  $x = 0$  and  $1$ , with the asymptotic behavior  $\phi_n^{M\overline{m}}(x) \rightarrow x^{\beta_M}$  as  $x \rightarrow 0$ , where

$$M_R^2 + \pi\beta_M \cot \pi\beta_M = 0, \quad (2.5)$$

and similarly as  $x \rightarrow 1$ , exchanging  $m$  for  $M$ .  $\beta_M$  is a monotonic function of  $M^2$  (or  $M_R^2$ ), increasing from zero to one as  $M^2 = 0 \rightarrow \infty$ .

Also useful in this description is the full meson-quark vertex  $\Phi_n^{M\bar{m}}$ , which is given by

$$\Phi_n^{M\bar{m}}(z) = \int_0^1 dy \phi_n^{M\bar{m}}(y) \operatorname{Pr} \frac{1}{(y-z)^2}, \quad (2.6)$$

for all complex values of  $z$ . Indeed, except for  $z \in [0,1]$ , the principal value prescription is unnecessary.

The decay constant  $f_n$  for meson  $n$  may be computed in this framework. It is given by

$$f_n = c_n / \sqrt{\pi}, \quad (2.7)$$

where

$$c_n \equiv \int_0^1 dx \phi_n(x). \quad (2.8)$$

Strictly speaking, the r.h.s. of (2.7) is also multiplied by a factor  $\sqrt{N_c}$ , but we may absorb this factor into the normalization of other factors by which it is multiplied in the full amplitudes; what is important is that the final physical amplitude has the correct  $N_c$  dependence at leading order. As each new quantity is calculated in this paper, we will point out the leading dependence on  $N_c$ , but as a rule we suppress the explicit factors for ease of notation. The 't Hooft eigenfunctions  $\phi_n$ , for example, are  $O(N_c^0)$  solutions of Eq. (2.4), and so  $c_n$  is also  $O(N_c^0)$ . On the other hand, light meson decay constants have the well-known behavior  $f_n \propto \sqrt{N_c}$ , and the full result Eq. (2.7), including the  $\sqrt{N_c}$ , may be verified by direct calculation.

The 't Hooft model wave functions  $\phi_n$  and  $\Phi_n$  are calculated by means of a standard numerical method called the Multhopp technique [12,15], in which the integral equation is converted to an equivalent infinite-dimensional eigenvalue system, which in turn may be truncated after a desired number of modes to give approximate wave function solutions. Since the relevant formulæ for unequal-mass mesons do not appear elsewhere, we present a summary in Appendix A.

Whereas the eigenfunctions  $\phi_n^{M\bar{m}}$  describe the complete set of homogeneous solutions for the two-point Green function, the solution for  $1 \rightarrow 2$  meson decays (the leading decay channels in large  $N_c$ ) requires also three-point Green functions. Remarkably, the requisite expressions may be written entirely in terms of triple overlap integrals of the functions  $\phi$  and  $\Phi$  [9,14], without bare quark model contact-type interactions. In physical terms, this means that the three vertices of the diagram for the three-point Green function are resonance dominated, without contact contributions. Nevertheless, for the diagrams computed, it will prove to be computationally convenient to describe part of the full amplitude in terms of these contact terms. We exhibit these explicit expressions in Sec. V, but for the moment it is only important to note that such expressions indeed exist.

### III. PECULIARITIES OF 1+1 DIMENSIONS

Despite one's hopes that exact calculations in the 't Hooft model may lend insight into real 3+1 strong interaction physics, we emphasize that the two-dimensional universe possesses some unique properties that must be remembered when comparing to the universe of

four dimensions. Therefore, the 't Hooft model may in no way be construed as any sort of limiting case of real QCD, and any direct comparisons are necessarily qualitative. In other words, we espouse the opinion that only certain conclusions based upon our numerical studies of 't Hooft model solutions, not the numerical results themselves, possess any validity in 3+1 dimensions.

The most obvious signal that 1+1 and 3+1 physics are vastly different is that the former does not possess the quantity of angular momentum, except in the residual form of parity<sup>1</sup>. This is clear since finite rotations do not exist when there is only one spatial direction, and only the improper “rotation” taking  $x^1 \rightarrow -x^1$ , namely parity, remains. It follows that 't Hooft model eigenstates  $\phi_n(x)$  do not possess spin, but only intrinsic parity  $(-1)^{n+1}$  [8]. All of the interesting phenomenology provided by approximate spin symmetries in our world (*i.e.*, the smallness of hyperfine splittings, relations between different helicity amplitudes, *etc.*) are therefore meaningless in two dimensions.

The lack of transverse directions has important consequences for couplings in 1+1 dimensions. As mentioned in the previous section, gauge couplings have dimensions of mass, and so such theories are super-renormalizable. Moreover, “vector” gauge bosons exist in 1+1 only through their longitudinal modes. There are also different Lorentz invariants in 1+1, since the Levi-Civita tensor  $\epsilon^{\mu\nu}$  has only two indices. The effects of these constraints are implicit in all the results to follow.

The amount of Lorentz-invariant phase space is of course expected to vary between different spacetime dimensions  $D$ , since the measure of the phase space integrals is the  $D$ -dimensional volume element. However, the difference between 1+1 and 3+1 is particularly dramatic. To be specific, in  $D$  spacetime dimensions, the differential width for a  $1 \rightarrow 2$  decay in terms of the solid angle of either final-state particle is given by

$$d\Gamma = \frac{|\mathbf{p}|^{D-3}}{(2\pi)^{D-2} 8M^2} |\mathcal{M}|^2 d\Omega, \quad (3.1)$$

where  $|\mathbf{p}|$  is the spatial momentum of either final-state particle in the rest frame of the initial particle of mass  $M$ , and  $\mathcal{M}$  is the invariant amplitude of the process. Note particularly the behavior of the phase space factor  $|\mathbf{p}|^{D-3}$  as the  $|\mathbf{p}| = 0$  threshold is approached: For  $D = 4$ , the differential width vanishes with the decreasing amount of phase space available, but for  $D = 2$ , the differential width actually becomes singular (barring an accidental zero in the amplitude  $\mathcal{M}$ ). It follows that two-particle decay modes near threshold are enhanced in 1+1, in stark contrast to 3+1.

#### IV. THE PARTONIC CALCULATION

Because of the small number of integrations necessary to compute phase space in 1+1 dimensions, it is possible to perform the partonic integrals analytically in all cases of interest

---

<sup>1</sup>Also, spinors retain the property of chirality, since a  $\gamma_5$  matrix still exists in 1+1, signaling two inequivalent representations of the Lorentz group.

to us. In the  $1 \rightarrow 3$  parton decay, one starts with  $3 \times 2 = 6$  final-state momentum components, of which 2 are fixed by energy-momentum conservation and 3 are fixed by the on-shell conditions of the final-state partons; this leaves only one nontrivial integration, which can be done explicitly.<sup>2</sup>

Here we consider the case of an initial quark of mass  $M$  decaying into three distinguishable equal-mass quarks of mass  $m \leq M/3$ . The final nontrivial integral involves a small number of square root factors arising from the on-shell mass-energy constraints, since both energies and momenta appear in both the phase space and the invariant amplitude expressed in a given frame. Such expressions in our case integrate to the standard three kinds of complete elliptic integrals of Legendre, usually denoted by  $K$ ,  $E$ , and  $\Pi$ . We begin by presenting the functional form for the phase space with constant invariant amplitude:

$$\Phi_3(M; m, m, m) = \frac{1}{4\pi^3 M^2} (1 + \epsilon)^{-1/2} (1 - \epsilon/3)^{-3/2} K(u), \quad (4.1)$$

where

$$\epsilon \equiv \frac{3m}{M} \in [0, 1], \quad (4.2)$$

and

$$u \equiv \sqrt{\frac{(1 - \epsilon)(1 + \epsilon/3)^3}{(1 + \epsilon)(1 - \epsilon/3)^3}}. \quad (4.3)$$

Note that, unlike the two-body phase space given by Eq. (3.1), this expression does not diverge for finite  $m$ . However, it does possess a singularity as  $m \rightarrow 0$  ( $\epsilon \rightarrow 0$ ), since then

$$\Phi_3 = \frac{3}{8\pi^3 M^2} \ln\left(\frac{M}{m}\right) \left[1 + O\left(\frac{m^2}{M^2}\right)\right]. \quad (4.4)$$

The opposite limiting case  $\epsilon \rightarrow 1$ , in which the three partons are produced at rest, is equally peculiar:

$$\Phi_3 = \frac{3\sqrt{3}}{32\pi^2 M^2} [1 + O(1 - \epsilon)], \quad (4.5)$$

which means that phase space does not vanish in this limit.

We now present the expressions for the inclusive partonic decay width. For definiteness, we attempt to describe the couplings in terms as similar to Standard Model (SM) notation as possible. Our labeling of partons is exhibited in Fig. 1. The decay of the heavy quark 1 to the lighter quark 3 is assumed to couple to a vector-like weak current with vertex

---

<sup>2</sup>Strictly speaking, there is also a degree of freedom from the “solid angle” of one of the final-state particles. However, in 1+1, this is a discrete degree of freedom. Integration of a differential width over this quantity gives an additional factor of  $1 + 1 = 2$  for Lorentz scalars and  $1 + (-1) = 0$  for pseudoscalars.

factor  $(-ig_2/\sqrt{2})V_{31}\gamma^\mu(c_V - c_A\gamma_5)$ , carried by a gauge boson “ $W$ ” of mass  $M_W$ ; in the SM,  $c_V = c_A = 1/2$ . The coupling at the other end of the weak current, creating quark 5 and antiquark 4, is assumed to be the same except for the “CKM element”  $V_{45}^*$ .  $G_F$  is defined, as in the SM, by  $\sqrt{2}g_2^2/8M_W^2$ ; note that  $G_F$  is dimensionless in 1+1. Finally, the abbreviations  $\epsilon$  and  $u$  are carried over from Eqs. (4.2) and (4.3).

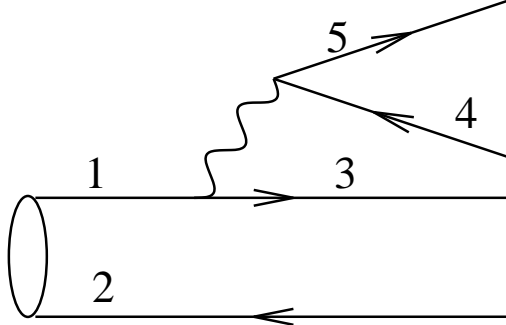


FIG. 1. *Parton decay diagram for the inclusive decay. Of interest are the parton labels, as used in the text.*

The weak decay amplitude and width in this case are effects of orders  $\sqrt{N_c}$  and  $N_c$ , respectively. This counting may be established in the parton diagram by observing that the pair  $(5\bar{4})$  in Fig. 1 can occur with each of the  $N_c$  colors, but “sewing up” the partons into color-singlet mesons  $(5\bar{4})$ ,  $(1\bar{2})$ , and  $(3\bar{2})$  costs a factor of  $1/\sqrt{N_c}$  each. Finally, each color may occur in the loop created by 1, 3, and 2, for one more factor of  $N_c$ . It follows that the weak decay width<sup>3</sup> calculated from the parton diagram is  $O(N_c)$ . In Sec. V we show that the hadronic calculation of the width also produces a leading factor of  $N_c$ .

The width is presented in two special cases. In the first, we take  $M_W \gg M$ , the usual four-fermion coupling assumption. This corresponds to using only the  $g_{\mu\nu}$  term in the numerator of the  $W$  propagator<sup>4</sup>,  $-i(g_{\mu\nu} - q_\mu q_\nu/M_W^2)/(q^2 + i\epsilon)$ . We then find

$$\Gamma = \frac{4G_F^2 M}{\pi} |V_{31} V_{45}^*|^2 (c_V^2 - c_A^2)^2 (1 - \epsilon/3)^{3/2} (1 + \epsilon)^{1/2} \times \left[ E(u) - 16(\epsilon/3)^3 (1 - \epsilon/3)^{-3} (1 + \epsilon)^{-1} K(u) \right]. \quad (4.6)$$

The limiting cases of this expression are given by

$$\Gamma \rightarrow \frac{4G_F^2 M}{\pi} |V_{31} V_{45}^*|^2 (c_V^2 - c_A^2)^2 \left[ 1 - \frac{\epsilon^2}{3} + O(\epsilon^3 \ln \epsilon) \right], \quad (4.7)$$

as  $\epsilon \rightarrow 0$ , and

---

<sup>3</sup>The difference from the strong width, which is  $O(1/N_c)$ , is that the  $q\bar{q}W$  vertices are unsuppressed in large  $N_c$ , while the  $q\bar{q}$ -gluon vertex is  $O(1/\sqrt{N_c})$ .

<sup>4</sup>We use unitary gauge in order to avoid the necessity of including additional charged Goldstone fields.

$$\Gamma \rightarrow \frac{16G_F^2 M}{3\sqrt{3}} |V_{31}V_{45}^*|^2 (c_V^2 - c_A^2)^2 (1 - \epsilon) \left[ 1 + \frac{3}{4}(1 - \epsilon) + O((1 - \epsilon)^2) \right], \quad (4.8)$$

as  $\epsilon \rightarrow 1$ . We see that the width is finite as  $\epsilon \rightarrow 0$  and vanishes as  $\epsilon \rightarrow 1$ . The former limit shows that the width for the partonic decay of the heavy quark is given approximately by  $M$  times a constant, dimensionless coefficient.

It is easy to understand the prefactor  $(c_V^2 - c_A^2)^2$ , which means that the width in the  $M_W \gg M$  limit vanishes for  $V \pm A$  currents. The decay vertex in this limit is of the form  $g^{\mu\nu} J_\mu j_\nu$  for some quark currents  $J$  and  $j$ . Note that the only non-vanishing components of the metric are  $g^{+-}$  and  $g^{-+}$ , so the vertex involves only  $J_- j_+$  and  $J_+ j_-$ . Now,  $V \pm A$  currents correspond to the quarks being all right(left)-handed. The currents  $J_\pm$  and  $j_\pm$  in this chiral basis are just bilinears of  $\gamma_\pm$ , since  $\gamma_\mu \gamma_5 \psi_{R,L} = \pm \gamma_\mu \psi_{R,L}$ . However, in  $1 + 1$  dimensions  $\gamma_- \psi_L = \gamma_+ \psi_R = 0$ , and so all currents of one chirality vanish, leading to the vanishing of the decay vertex.

If we impose  $c_V^2 = c_A^2 = 1/4$  from the beginning of the calculation, then we find that only pieces obtained from contraction with the  $q_\mu q_\nu$  terms in the  $W$  propagator survive, giving rise to the width

$$\begin{aligned} \Gamma = & \frac{G_F^2 M^5}{\pi M_W^4} |V_{31}V_{45}^*|^2 (\epsilon/3)^2 (1 - \epsilon/3)^{-3/2} (1 + \epsilon)^{-1/2} \\ & \times \left\{ -8(\epsilon/3)^2 \left[ (1 + \epsilon/3)^3 + (\epsilon/3)(1 - \epsilon/3)^2 \right] K(u) \right. \\ & + \left( 1 + \epsilon^2/9 \right) (1 - \epsilon/3)^3 (1 + \epsilon) E(u) \\ & \left. + 48(\epsilon/3)^3 \left( 1 + \epsilon^2/27 \right) \Pi(v, u) \right\}, \end{aligned} \quad (4.9)$$

where

$$v \equiv \frac{(1 + \epsilon/3)(1 - \epsilon)}{(1 - \epsilon/3)(1 + \epsilon)}. \quad (4.10)$$

The asymptotic expansions in this case are

$$\Gamma \rightarrow \frac{G_F^2 M^5}{\pi M_W^4} \left( \frac{\epsilon}{3} \right)^2 \left[ 1 - \frac{2\epsilon^2}{9} + O(\epsilon^3) \right], \quad (4.11)$$

for  $\epsilon \rightarrow 0$ , and

$$\Gamma \rightarrow \frac{8G_F^2 M^5}{243\sqrt{3}M_W^4} \left[ 1 + \frac{1}{2}(1 - \epsilon) + O((1 - \epsilon)^2) \right], \quad (4.12)$$

for  $\epsilon \rightarrow 1$ . Here we see that the width vanishes as  $\epsilon \rightarrow 0$  but is finite as  $\epsilon \rightarrow 1$ . Specifically, in the former limit the width is approximately a dimensionless constant times  $M^3 m^2 / M_W^4$ .

## V. THE HADRONIC CALCULATION

Matrix elements for exclusive  $1 \rightarrow 2$  meson decays are most conveniently written in terms of transition form factors. We identify the  $\bar{B}$  meson in  $1+1$  as the ground state of

the  $M\bar{m}$  tower of resonances to which it belongs, and subsequently label it by **0**. Consider the “tree” (T) diagram of Fig. 2, for which  $\bar{B} = (1\bar{2})$ , where 1 is the heavy “ $b$ ” quark; the matrix element is parameterized by

$$\langle \mathbf{m}(p') | \bar{q}\gamma^\mu Q | \mathbf{0}(p) \rangle = \begin{cases} (p + p')^\mu f_+(q^2) + (p - p')^\mu f_-(q^2) & \text{for } m \text{ even,} \\ \epsilon_{\mu\nu}(p + p')^\nu f_+(q^2) + \epsilon_{\mu\nu}(p - p')^\nu f_-(q^2) & \text{for } m \text{ odd,} \end{cases} \quad (5.1)$$

where  $q^2 \equiv (p - p')^2$ , and  $Q$  and  $q$  indicate the fields of quarks with masses  $M$  and  $m$ . The light quark field  $q$  here refers to the daughter of the heavy quark (3 in Fig. 2), not the spectator quark (2 in Fig. 2), although both are taken to have mass  $m$ . The label  $\mathbf{m}$  indicates the eigenvalue index of the final-state decay product meson  $(2\bar{3})$  not coupled to the flavor-changing current. In the remainder of this section,  $m$  exclusively means this value and not the value of the light quark mass.

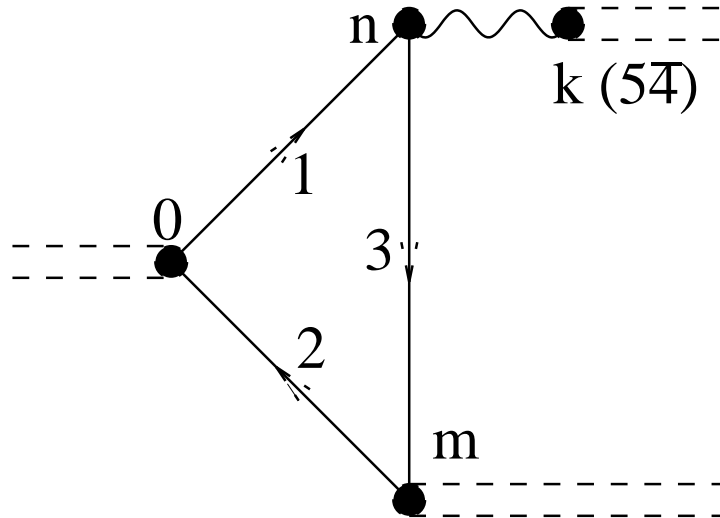


FIG. 2. Diagram for “tree” (T) meson exclusive decay. Numbers indicate quark labels used in the text (except **0**, which refers to the ground-state  $\bar{B}$  meson), while letters indicate the eigenvalue index of meson resonances. One can also consider contact-type diagrams, in which the point labeled by **n** is not coupled to a resonance.

Next, we reserve the label **n** in the T diagram for the meson resonances or contact terms  $(1\bar{3})$  coupled to the flavor-changing current. **n** carries the momentum transfer  $q^2$ , which is the kinematic variable of interest in this system; however, it proves more convenient to use the equivalent Lorentz-invariant quantity  $\omega \equiv p_-/q_-$ , which indicates the fraction of light-cone coordinate “spatial” component of the current  $q_-$  carried by meson **0**. In the method of calculating the matrix element (5.1) developed in [12], one considers not **0**  $\rightarrow \mathbf{mn}$  directly, but rather the crossed process **n**  $\rightarrow \mathbf{0}\bar{m}$  above its threshold ( $q^2 \geq (\mu_0 + \mu_m)^2$ ); in that case, one finds  $\omega \in [0, 1]$ :

$$\omega(q^2) = \frac{1}{2} \left[ 1 + \left( \frac{\mu_0^2 - \mu_m^2}{q^2} \right) - \sqrt{1 - 2 \left( \frac{\mu_0^2 + \mu_m^2}{q^2} \right) + \left( \frac{\mu_0^2 - \mu_m^2}{q^2} \right)^2} \right]. \quad (5.2)$$

Here and below we use the same symbol  $\mu$  for the masses of heavy-light and light-light mesons, since from the index one can immediately tell which one is appropriate (*e.g.*,  $\mu_0$  is

heavy-light). Since  $\omega$  is obtained by solving the quadratic equation  $q^2\omega^2 + (\mu_m^2 - \mu_0^2 - q^2)\omega + \mu_0^2 = 0$ , it should be pointed out that the branch choice used for  $\omega$  does not affect the final numerical results for form factors or amplitudes; the two branches simply correspond to the two possible directions of the mesons **0** and **1̄m** in the rest frame of **n**. However, the branch chosen above turns out to greatly facilitate the numerical computations. For some values of  $q^2$  below this crossed-process threshold,  $\omega$  is complex, and the following expressions for the form factors must be computed in a different way, as discussed below.

With the aforementioned identifications, we may express the form factors entirely in terms of resonance quantities, as promised in Sec. II. The notation and form factor expressions we present here appear in Ref. [14], while the characteristic integral expression contained within was first obtained in [9]. The form factors are explicitly

$$f_+(q^2) = \sum_n \frac{\mathcal{A}_n(q^2)}{1 - q^2/\mu_n^2}, \quad (5.3)$$

and

$$f_-(q^2) = \frac{1}{q^2} \left[ \sum_n \frac{\mathcal{B}_n(q^2)}{1 - q^2/\mu_n^2} - \sum_n \frac{\mathcal{A}_n(q^2)}{1 - q^2/\mu_n^2} (\mu_0^2 - \mu_m^2) \right], \quad (5.4)$$

where the pole residue functions  $\mathcal{A}_n$  and  $\mathcal{B}_n$  are given by

$$\mathcal{A}_n(q^2) = \frac{c_n [1 + (-1)^{n+m}]}{(q^2\omega - \mu_0^2/\omega)} F_{n0m}(\omega), \quad (5.5)$$

and

$$\mathcal{B}_n(q^2) = c_n [1 + (-1)^{n+m+1}] F_{n0m}(\omega), \quad (5.6)$$

and the triple overlap integral  $F_{n0m}$  is defined by

$$F_{n0m}(\omega) \equiv \left[ \frac{1}{1 - \omega} \int_0^\omega dv \phi_n^{1\bar{3}}(v) \phi_0^{1\bar{2}}\left(\frac{v}{\omega}\right) \Phi_m^{2\bar{3}}\left(\frac{v - \omega}{1 - \omega}\right) - \frac{1}{\omega} \int_\omega^1 dv \phi_n^{1\bar{3}}(v) \Phi_0^{1\bar{2}}\left(\frac{v}{\omega}\right) \phi_m^{2\bar{3}}\left(\frac{v - \omega}{1 - \omega}\right) \right]. \quad (5.7)$$

We now compute the invariant matrix element for a current coupling of the form  $(-ig_2/\sqrt{2})V_{31}\gamma^\mu (c_V - c_A\gamma_5)$ , exactly as for the inclusive decay. Such a calculation is possible for an arbitrary combination of  $V$  and  $A$  currents, even though we presented the matrix element only for a current of the bilinear  $V^\mu \equiv \bar{q}\gamma^\mu Q$ , because the two currents are related by  $\gamma_\mu\gamma_5 = \epsilon_{\mu\nu}\gamma^\nu$ . The invariant matrix element is simply the product of a linear combination of the form factors determined by the current coupling, multiplied by the propagator of the flavor-changing current (the “ $W$ ”) and finally by a factor representing the meson formed from the flavor-changing current. The last step amounts, via LSZ reduction of the two-point Green function, to the insertion of a factor of the meson decay constant. In the T diagram, we assign this meson the label **k** and quark structure (54). Using Eq. (2.7) to write the decay constant  $f_k$  in terms of  $c_k$ , we have at last

$$\begin{aligned}
\mathcal{M}_T = & c_k \sqrt{\frac{2}{\pi}} \frac{G_F M_W^2}{(M_W^2 - q^2)} V_{31} V_{45}^* \\
& \cdot \sum_n \left\{ 2 \left[ (c_V^2 - c_A^2) \left( (-1)^k + (-1)^n \right) \right] \right. \\
& \quad \left. + \frac{q^2}{M_W^2} \left[ (c_V + c_A)(-1)^k - (c_V - c_A) \right] \left[ (c_V + c_A)(-1)^n - (c_V - c_A) \right] \right\} \\
& \cdot \frac{c_n \mu_n^2}{q^2 - \mu_n^2} F_{n0m}(\omega), \tag{5.8}
\end{aligned}$$

where the on-shell process has  $q^2 = \mu_k^2$ . The pseudoscalar parity of the ground state  $\bar{B}$  has been taken into account in this expression. We remind the reader that in this expression  $F_{n0m}$  is given by (5.7) only for  $n$  such that  $\mu_n^2 > (\mu_0 + \mu_m)^2$ ; other methods must be employed for smaller  $\mu_n^2$ , as described below.

The conversion of the decay constant  $f_k$  to  $c_k$  in fact gives the only surviving factor of  $\sqrt{N_c}$  in the amplitude, which means that the weak decay width is proportional to  $N_c$ , in agreement with the partonic result of Sec. IV. This may be seen with reference to Fig. 2 by the usual large  $N_c$  counting arguments: The coupling of three mesons (**0**, **m**, and **n** in this case) appears with the factor  $1/\sqrt{N_c}$ , while meson **n** is destroyed by the  $W$  current, thus providing a decay constant at  $O(\sqrt{N_c})$ . This part of the diagram alone, which is none other than the form factors  $f_{\pm}(q^2)$ , is thus  $O(N_c^0)$ . The creation of the meson **k** from the weak current gives the remaining factor of  $\sqrt{N_c}$ . Finally, the width is given by Eq. (3.1).

The question remains what to do with the contributions from current-coupled resonances below the thresholds for the T diagram. The expressions listed above are inadequate because they assume the reality of  $\omega$  in the computation of contour integrals with denominators of the form  $(\omega + c \pm i\varepsilon)$ , where the  $\varepsilon$  arises from the Feynman prescription in the fermion propagators, and  $c$  represents other purely real numbers arising from the loop calculation. Such integrals are naturally trivial when  $\omega$  is real and simply lead to step functions. However, when  $\omega$  is complex the results are rather more cumbersome (although still tractable in principle). One may resort instead to other methods [12] in order to obtain amplitudes from the below-threshold resonances. The approach relies on sum rules [9] that are satisfied by the amplitudes, and are described in Appendix B. The upshot is that the sum rules may be used to describe the below-threshold amplitudes in terms of combinations of values from the above-threshold amplitudes, a process to which we refer as “backsolving”.

However, backsolving has drawbacks from the practical point of view. As the number of resonances below threshold increases, the number of the above-threshold pole residues and corresponding accuracies with which these are computed must increase dramatically to maintain the accuracy of the below-threshold residues thus calculated. For transitions of the  $\bar{B}$  meson to light  $\pi$ 's, it is known [12,14] that the below-threshold pole residues are very large compared to their above-threshold fellows, and tend to alternate in sign. Clearly, a small uncertainty in the above-threshold calculation magnifies to a large uncertainty in the below-threshold residues, and the alternating sign suggests delicate cancellations among the computed residues, which makes the situation even worse.

There is a much more efficient method of calculation if we are willing to abandon the requirement that all vertices in the calculation of Fig. 2 are resonant couplings, and allow for quark model-type contact terms. The calculation is based upon the observation that  $\omega$  as

defined in Eq. (5.2) is real not only for decays in the crossed kinematic region  $q^2 \geq (\mu_0 + \mu_m)^2$ , but also decays in the direct decay kinematic region  $0 \leq q^2 \leq (\mu_0 - \mu_m)^2$ , where  $\omega \geq 1$ . It therefore makes sense to redefine  $\omega \equiv q_-/p_-$  rather than  $p_-/q_-$ , so that  $\omega \in [0, 1]$  in this range. One then finds

$$\omega(q^2) = \frac{1}{2} \left[ 1 + \left( \frac{q^2 - \mu_m^2}{\mu_0^2} \right) - \sqrt{1 - 2 \left( \frac{q^2 + \mu_m^2}{\mu_0^2} \right) + \left( \frac{q^2 - \mu_m^2}{\mu_0^2} \right)^2} \right]. \quad (5.9)$$

It is convenient to define the triple overlap integral

$$F_{0nm}(\omega) \equiv \left[ \frac{1}{1-\omega} \int_0^\omega dv \phi_0^{1\bar{2}}(v) \phi_n^{1\bar{3}}\left(\frac{v}{\omega}\right) \Phi_m^{3\bar{2}}\left(\frac{v-\omega}{1-\omega}\right) - \frac{1}{\omega} \int_\omega^1 dv \phi_0^{1\bar{2}}(v) \Phi_n^{1\bar{3}}\left(\frac{v}{\omega}\right) \phi_m^{3\bar{2}}\left(\frac{v-\omega}{1-\omega}\right) \right], \quad (5.10)$$

as well as the contact terms

$$\begin{aligned} \mathcal{C}_1 &\equiv -\frac{1}{\omega} \int_\omega^1 dv \phi_0^{1\bar{2}}(v) \phi_m^{3\bar{2}}\left(\frac{v-\omega}{1-\omega}\right), \\ \mathcal{C}_2 &\equiv -\omega \int_\omega^1 dv \phi_0^{1\bar{2}}(v) \phi_m^{3\bar{2}}\left(\frac{v-\omega}{1-\omega}\right) \frac{1}{v(v-\omega)}, \\ \mathcal{C}_3 &\equiv -\frac{1}{1-\omega} \int_0^\omega dv \phi_0^{1\bar{2}}(v) \Phi_m^{3\bar{2}}\left(\frac{v-\omega}{1-\omega}\right). \end{aligned} \quad (5.11)$$

Note that the triple overlap is somewhat different from that in Eq. (5.7), both in the arguments of each wave function and the definitions ((5.2) and (5.9)) of  $\omega$  for each case. Furthermore, there is some flexibility in how one expresses results containing these contact terms, since one can use the completeness of the 't Hooft model eigenfunctions on  $x \in [0, 1]$  to show  $\sum_n c_n \phi_n(x) = 1$ , and from this prove identities such as

$$\sum_n c_n F_{0nm}(\omega) = \mathcal{C}_2 - \mathcal{C}_3. \quad (5.12)$$

After a lengthy but straightforward calculation, one finds

$$f_+(q^2) = \sum_n \frac{\mathcal{A}_n(q^2)}{1 - q^2/\mu_n^2} + \frac{1}{(q^2/\omega - \mu_0^2\omega)} \left\{ q^2 \mathcal{C}_1 - [1 + (-1)^m m_1 m_3] \mathcal{C}_2 + \mathcal{C}_3 \right\}, \quad (5.13)$$

and

$$\begin{aligned} f_-(q^2) &= \frac{1}{q^2} \left\{ \sum_n \frac{\mathcal{B}_n(q^2)}{1 - q^2/\mu_n^2} - \sum_n \frac{\mathcal{A}_n(q^2)}{1 - q^2/\mu_n^2} (\mu_0^2 - \mu_m^2) \right. \\ &\quad \left. + (1-r) (q^2 \mathcal{C}_1 - \mathcal{C}_3) - \left[ [1 + (-1)^{m+1}] - [1 + (-1)^m] m_1 m_3 r \right] \mathcal{C}_2 \right\}, \end{aligned} \quad (5.14)$$

where

$$r \equiv \frac{\mu_0^2 - \mu_m^2}{q^2/\omega - \mu_0^2\omega}, \quad (5.15)$$

and the pole residue functions are given by (compare (5.3) and (5.4))

$$\mathcal{A}_n(q^2) = \frac{c_n [1 + (-1)^{n+m}]}{(q^2/\omega - \mu_0^2\omega)} F_{0nm}(\omega), \quad (5.16)$$

and

$$\mathcal{B}_n(q^2) = c_n [1 + (-1)^{n+m+1}] F_{0nm}(\omega). \quad (5.17)$$

Finally, the matrix element for the decay  $\mathbf{0} \rightarrow \mathbf{m}\mathbf{k}$ , which unlike Eq. (5.8) holds for all such decays allowed by kinematics, is given by

$$\begin{aligned} \mathcal{M}_T = c_k \sqrt{\frac{2}{\pi}} \frac{G_F M_W^2}{(M_W^2 - q^2)} V_{31} V_{45}^* & \cdot \left[ 2(c_V^2 - c_A^2) \left\{ \sum_n \frac{[(-1)^k q^2 + (-1)^n \mu_n^2] c_n}{q^2 - \mu_n^2} F_{0nm}(\omega) + (-1)^{k+1} q^2 \mathcal{C}_1 + m_1 m_3 \mathcal{C}_2 \right\} \right. \\ & + \frac{q^2}{M_W^2} [(c_V + c_A)(-1)^k - (c_V - c_A)] \\ & \cdot \left\{ \sum_n \frac{c_n}{q^2 - \mu_n^2} [(c_V + c_A)(-1)^n \mu_n^2 - (c_V - c_A)q^2] F_{0nm}(\omega) \right. \\ & \left. \left. + (c_V - c_A)q^2 \mathcal{C}_1 + (c_V + c_A)m_1 m_3 \mathcal{C}_2 \right\} \right], \end{aligned} \quad (5.18)$$

where as before,  $q^2 = \mu_k^2$ .

## VI. RESULTS AND DISCUSSION

We computed the weak decay width of a free heavy quark with masses  $M = 2.28 \rightarrow 15.00$  in units of  $g\sqrt{N_c/2\pi}$  using Eq. (4.6), the  $M_W \rightarrow \infty$  case. Likewise, we computed the hadronic width using the same range of heavy quark mass and a fixed light quark mass  $m = 0.56$ . The expressions used were Eqs. (5.18) and (3.1), with definitions (2.8), (5.9), (5.10), (5.11), and with sums over all channels  $\mathbf{0} \rightarrow \mathbf{m}\mathbf{k}$  satisfying the on-shell condition  $\mu_m + \mu_k \leq \mu_0$ . Both widths are taken to have the same overall multiplicative factor  $2G_F^2 |V_{31} V_{45}^*|^2 (c_V^2 - c_A^2)^2 / \pi$ .

It is equally possible, in principle, to use (5.8) instead of (5.18) and backsolve for pole residues  $\mathcal{A}_n$  and  $\mathcal{B}_n$  defined in (5.5)–(5.6), or equivalently the overlap integrals  $F_{n0m}$ , using the expressions in Appendix B whenever  $\mu_n < \mu_0 + \mu_m$ , and obtain the hadronic width in this way. However, as discussed in Sec. V, this approach rapidly leads to uncontrollably large numerical uncertainties. Nevertheless, we were able to show in some simple cases with only a few backsolved residues that both methods produce the same numerical result within a few percent.

It is no more difficult to consider cases other than  $M_W \rightarrow \infty$ . For example, if one imposes the condition  $V - A$  condition  $c_V = c_A = 1/2$ , then Eq. (5.18) is just as valid, but now one uses the partonic width (4.9).

Of course, the partonic width is just a single easily evaluated function of the quark masses. The hadronic width, on the other hand, requires first the solution of the 't Hooft

equation, which is accomplished by means of the Multhopp technique described in Appendix A, repeated for as many resonances as desired. Next, the matrix elements are obtained by taking sums of overlap integrals over these wave functions, as in Eqs. (5.10) and (5.11). We compute the first 500 eigenvectors but include only the first 50 in our sums over resonances. The results change very little when more resonances are included. Finally, the amplitude for a given exclusive process is squared and multiplied by phase space to give the hadronic width.

Clearly, such a procedure uses a significant amount of computing time, and therefore it is not practical to compute the hadronic width at points exceptionally finely spaced in  $M$ . In practice, we computed each above-threshold amplitude at values of  $M = 2.28$  and each integer mass from  $M = 3.00$  to  $15.00$ . The significance of the lower bound is that, with the given light quark mass  $m = 0.56$ , this “ $b$  quark” mass gives a ground-state “ $\bar{B}$ ” meson just above the threshold for producing two ground-state “ $\pi$ ” mesons, *i.e.*, the smallest value of heavy quark mass unstable under hadronic weak decay.

We then make the empirical observation that the amplitudes for exclusive processes  $\mathcal{M}_T(\mathbf{0} \rightarrow \mathbf{mk})$  are smooth functions of  $M$ . We thus obtain the value of the amplitude at all intermediate points  $M$  by fitting to a fixed power law behavior over each interval, either by interpolating for values between adjacent pairs of points where the amplitudes were computed directly, or by extrapolating from the nearest two points if we are probing values of  $M$  above the process threshold but below the first explicitly computed point. In fact, we find that the exclusive amplitudes do not vanish at threshold and are usually<sup>5</sup> monotonically increasing functions of  $M$  (for example, see Fig. 3), although the rate of this increase is dependent upon the particular exclusive mode under consideration. The phase space is a known function of the computed meson masses, and thus the width can be reliably computed at any value of  $M$  in the desired range.

---

<sup>5</sup>In the few exceptions to this rule, the amplitude dips slightly for values of  $M$  just above threshold, but thenceforth assumes monotonically increasing behavior.

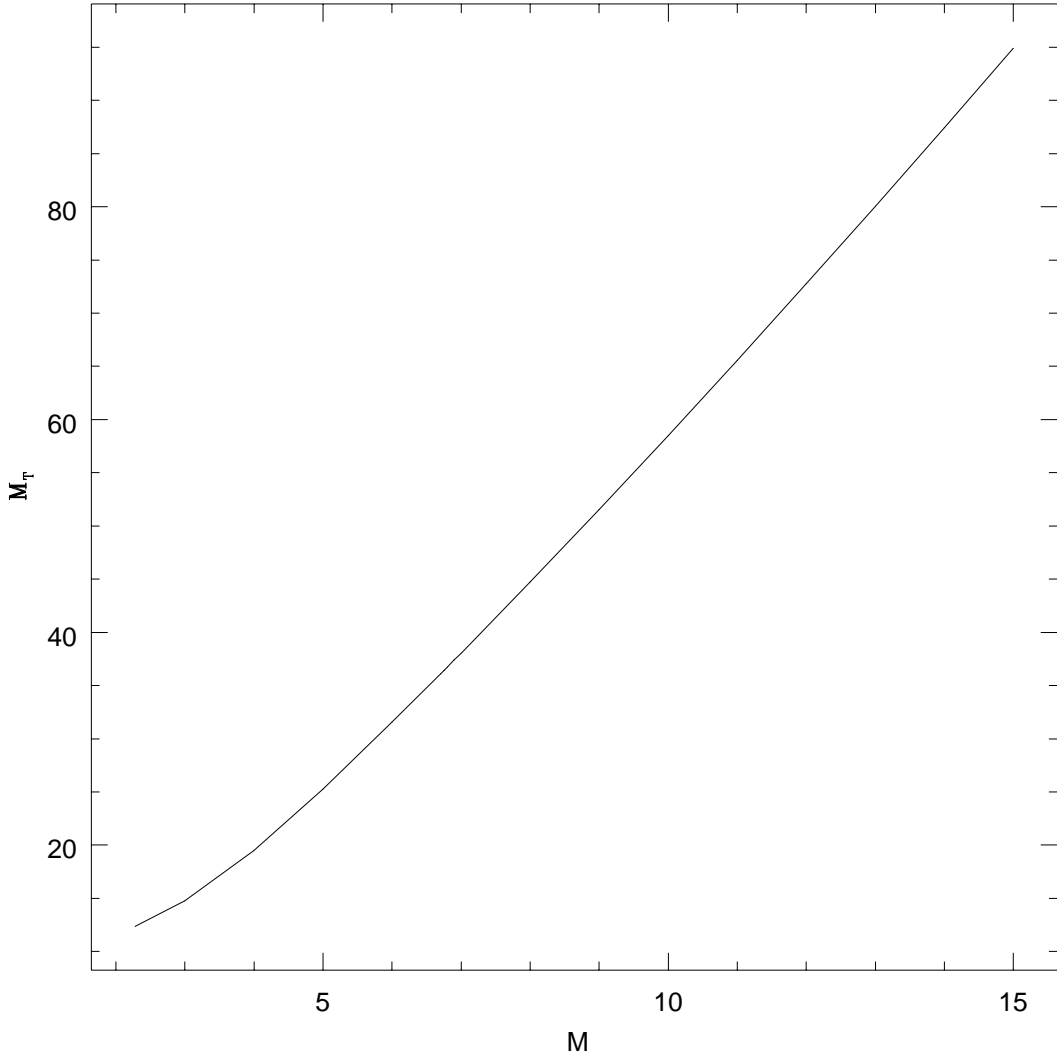


FIG. 3. Weak decay amplitude  $M_T$  for the exclusive decay to the lowest mode  $\mathbf{0} \rightarrow (\mathbf{m} = 0), (\mathbf{k} = 0)$ , as a function of heavy quark mass  $M$ , with light quark mass  $m = 0.56$ . The overall factor  $2\sqrt{2/\pi} G_F V_{31} V_{45}^* (c_V^2 - c_A^2)$  in the amplitude is suppressed for convenience.

Since the phase space in 1+1 is singular at threshold (Eq. (3.1)), one would expect a plot of width  $\Gamma$  vs.  $M$  to be very ill-behaved, with dramatic singularities increasing in density as  $M$  increases. One would expect it to be essential to use some sort of smearing in  $M$  to properly test duality between this hadronic description of the  $\Gamma$  and the smooth partonic result. In fact, this does not appear to be the case. We refer to Fig. 4, which is our central result. It is obtained by interpolating each exclusive decay amplitude, as described above, at intervals of  $\Delta M = 0.01$ . The remarkable result is that, after passing the first couple of thresholds,  $\Gamma$  appears to be a nearly smooth function in  $M$ , barely sensitive to the phase space singularities as each new threshold is passed. This result suggests that the effect of individual higher resonances is quite minimal, as one might expect in 3+1 dimensions. In

the 1+1 case, however, the result is all the more surprising, since now phase space near threshold provides a large enhancement rather than a suppression.

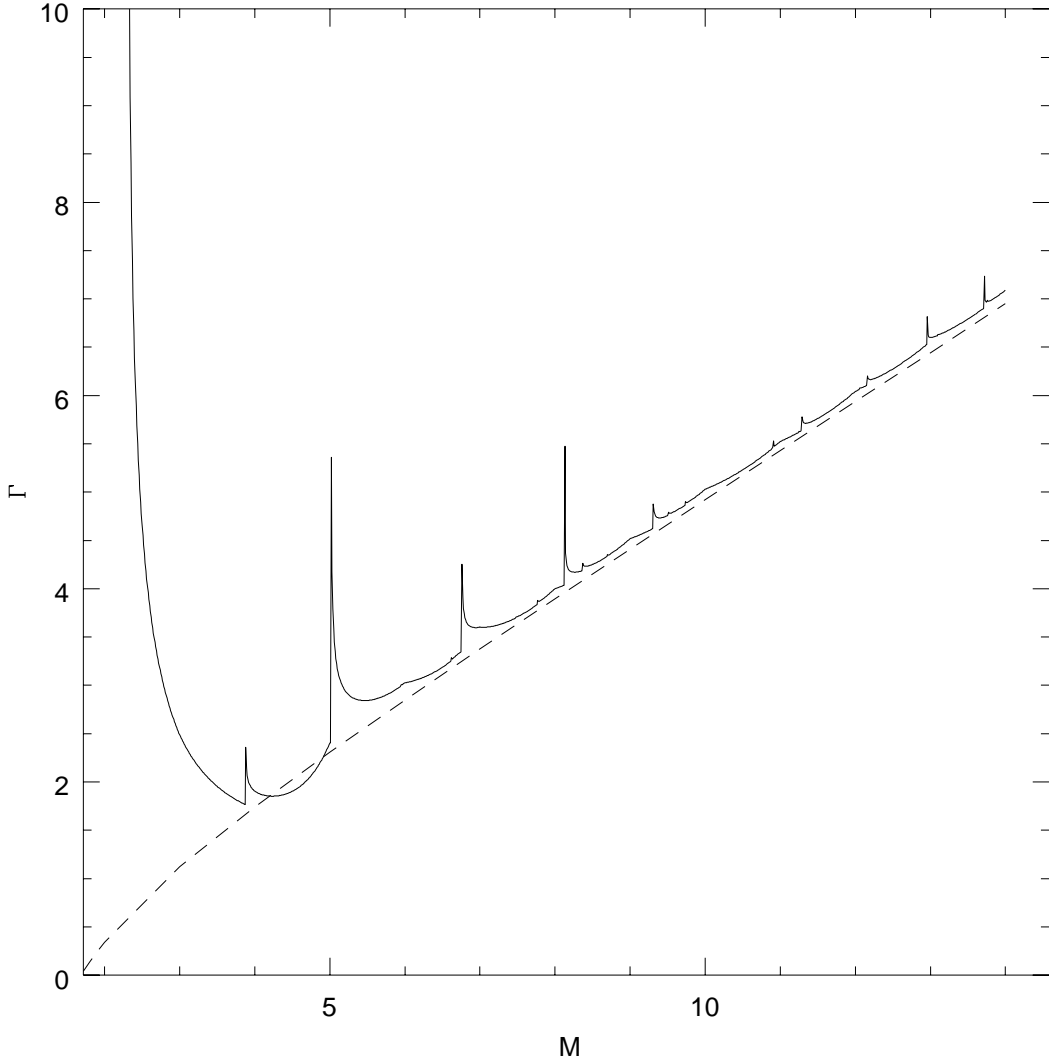


FIG. 4. The full decay width for the sum of exclusive modes in the decay  $\mathbf{0} \rightarrow \mathbf{m}\mathbf{k}$  as a function of heavy quark mass  $M$ , with light quark mass  $m = 0.56$ . The overall factor  $8G_F^2|V_{31}V_{45}^*|^2(c_V^2 - c_A^2)^2/\pi$  in the width is suppressed for convenience. The dashed line is the tree-level parton result, Eq. (4.6).

It is interesting to watch the width develop as more and more resonances are added. In Figs. 5a–5d we include exclusive channels with the lowest 1, 3, 5, and 11 thresholds, respectively. We now see explicitly that the full width over the range in  $M$  we consider is essentially produced by the first 11 channels, indicating the decreasing influence of individual higher resonances. The small wave in  $\Gamma$  above all the included thresholds is an artifact due to the interpolation routine between values of  $M$  at which the amplitudes are explicitly computed; its small size indicates the smoothness of the amplitudes in  $M$  and the reliability

of the interpolation.

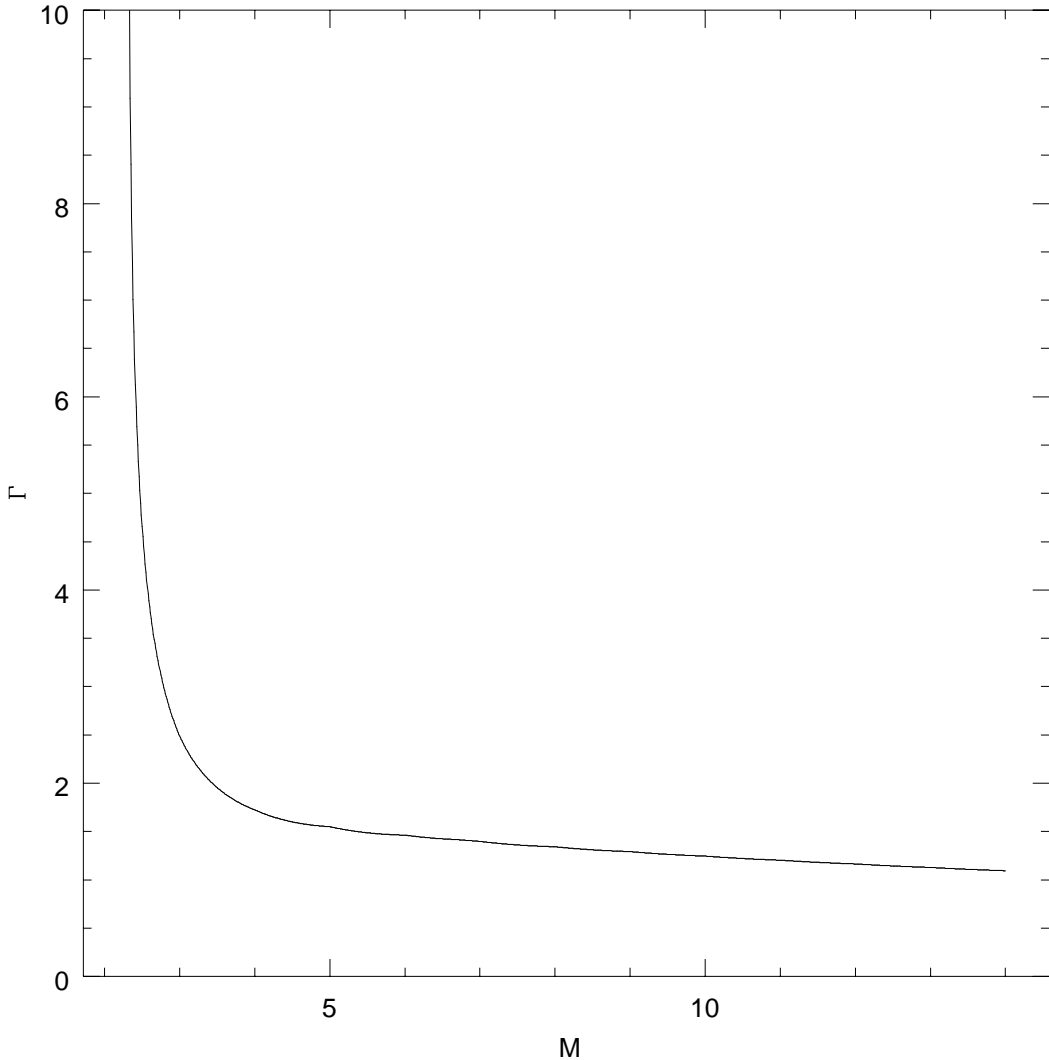


FIG. 5a. The full decay width as a function of heavy quark mass  $M$ , with light quark mass  $m = 0.56$ , including only the exclusive mode with the lowest threshold value (corresponding to  $\mathbf{m} = \mathbf{k} = 0$ ). The scale is the same as in Fig. 4.

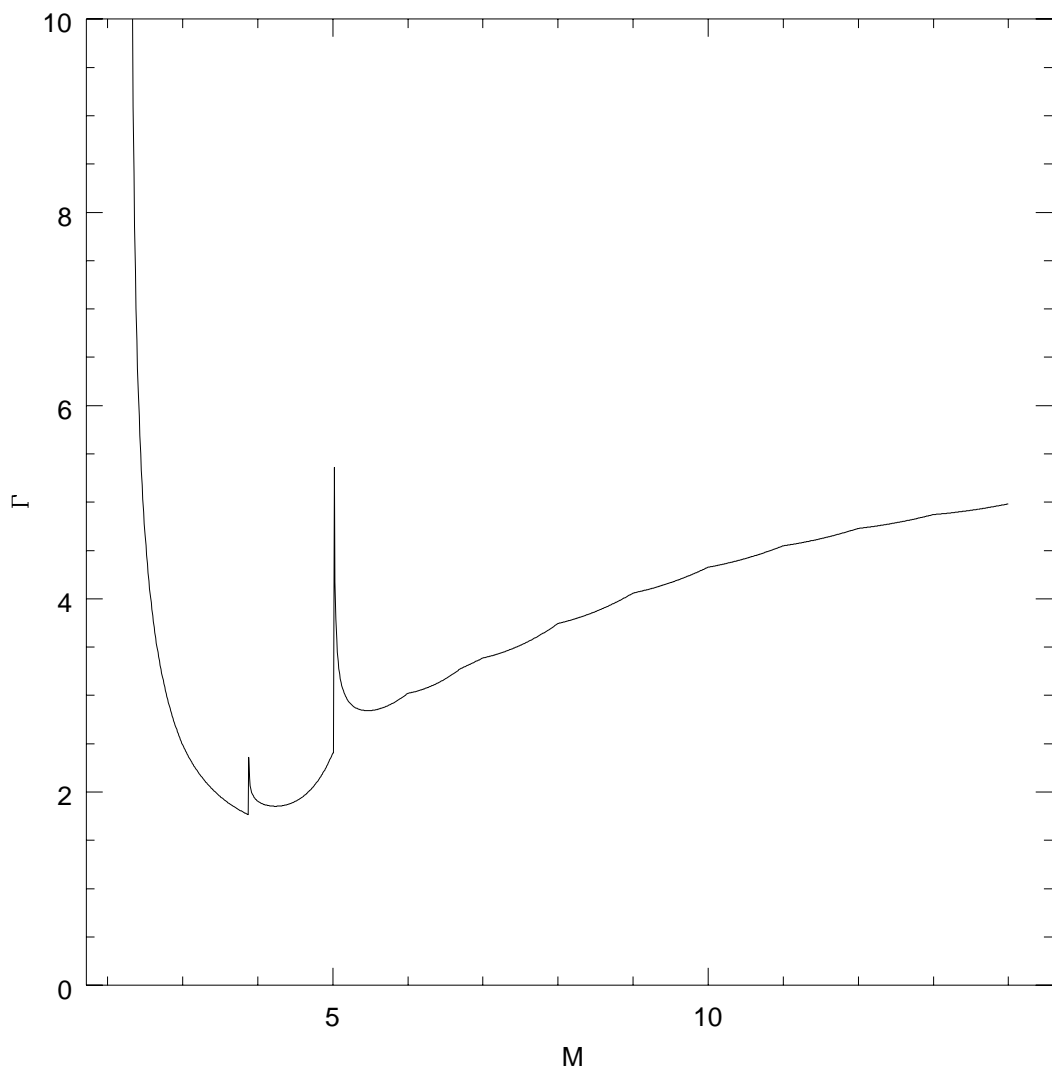


FIG. 5b. Same as Fig. 5a, except now including the exclusive modes corresponding to the three lowest threshold values.

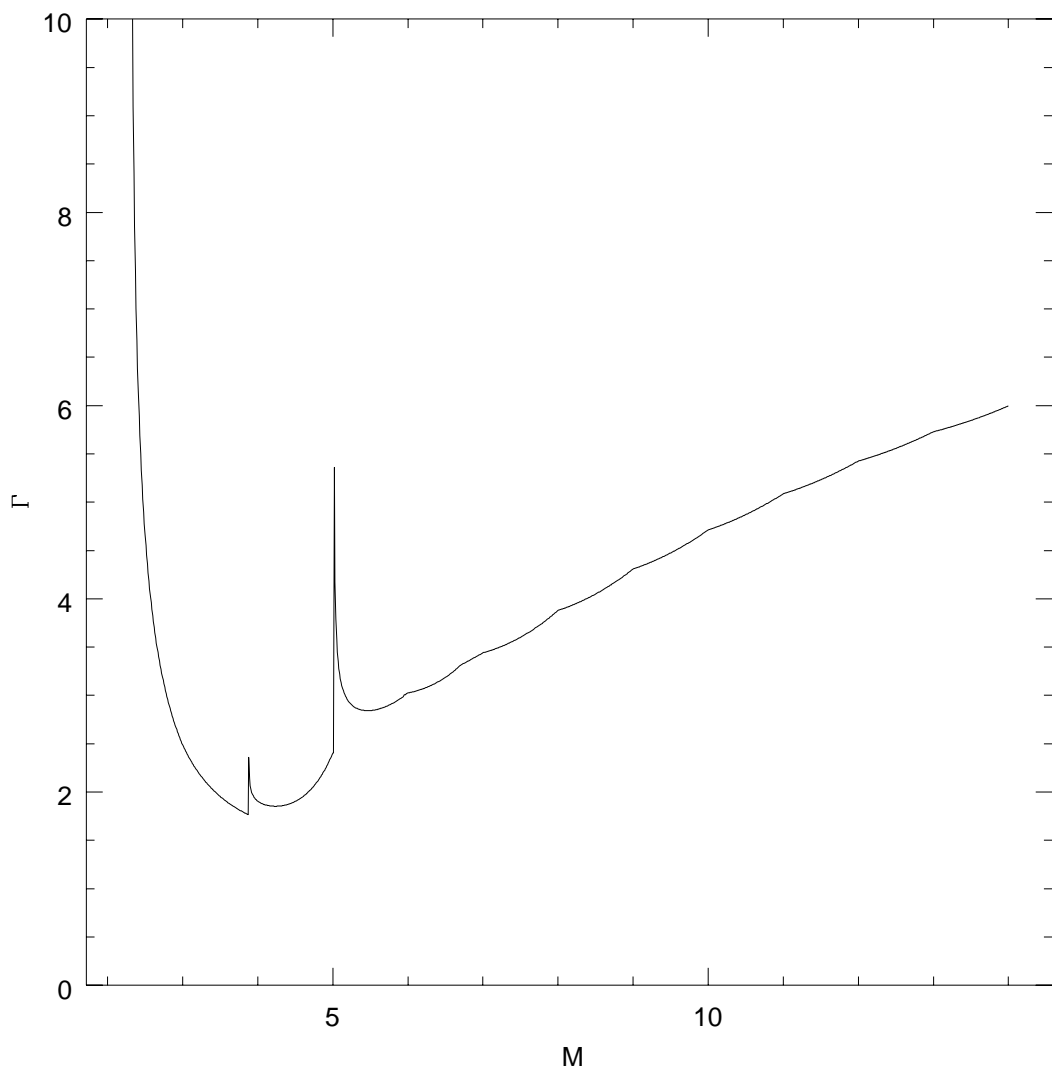


FIG. 5c. Same as Fig. 5a, except now including the exclusive modes corresponding to the five lowest threshold values.

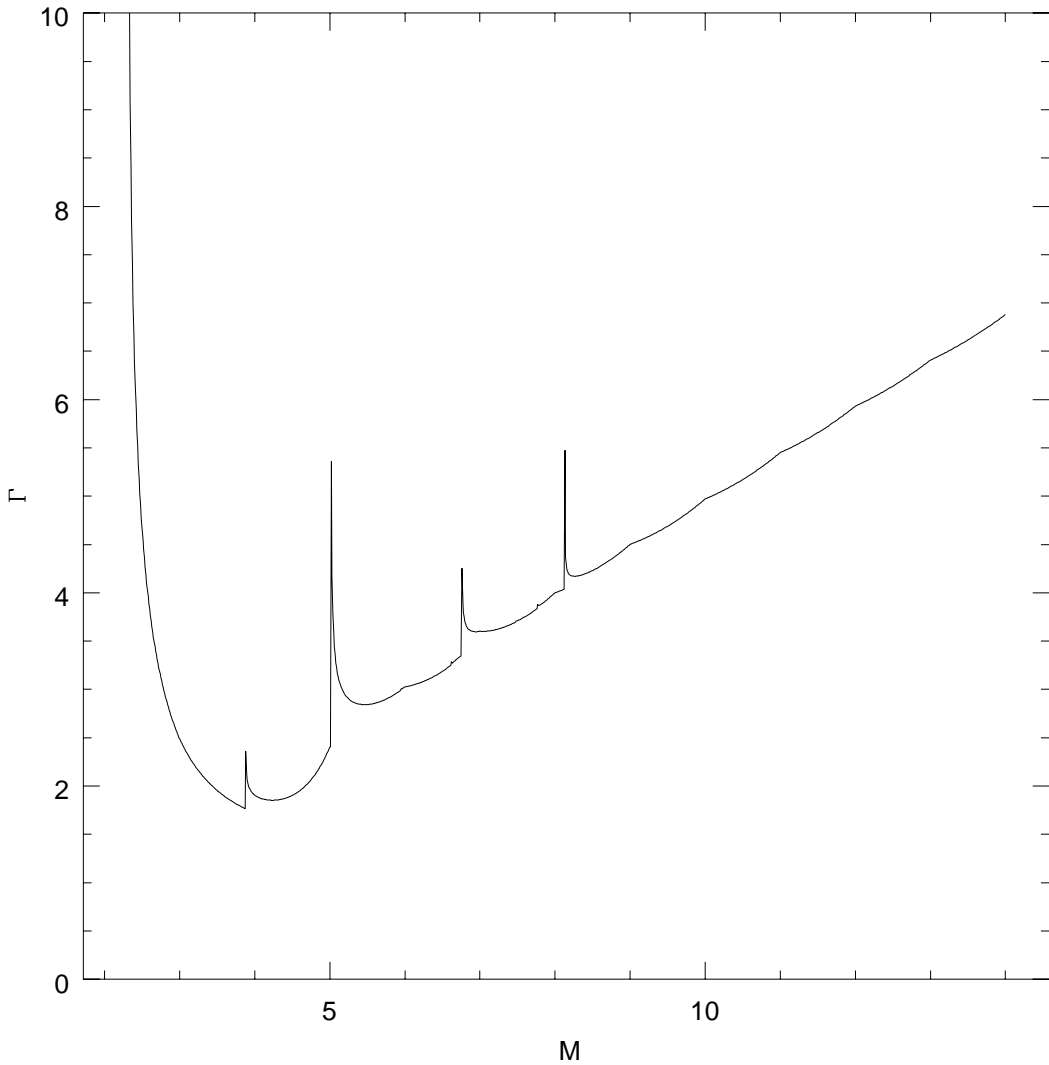


FIG. 5d. Same as Fig. 5a, except now including the exclusive modes corresponding to the eleven lowest threshold values. Observe that this figure is almost indistinguishable from the full result, Fig. 4.

Another remarkable feature of Fig. 4 is the near-perfect linearity of  $\Gamma$  for values  $M > 7.0$ . Suppressing the proportionality constant between  $\Gamma$  and  $M$ , Fig. 4 appears to obey the asymptotic form  $\Gamma \approx 0.514M - 0.141$ . This is surprisingly close to what is predicted asymptotically for the partonic rate: Suppressing the same proportionality constant in Eq. (4.7), one predicts  $\Gamma_{\text{part}} = \frac{1}{2}M(1 + O(1/M^2))$ .

One may ask whether the strength of the peaks in Fig. 4 is large enough that the mass-smeared partonic and hadronic widths nevertheless disagree. That is, local duality appears remarkably well satisfied, but perhaps global duality actually fails by concealing a large portion of  $\Gamma(M)$  in the very narrow threshold peaks. In this scenario, the apparent asymptotic smoothness of Fig. 4 fools us, for the density of threshold singularities increases with  $M$  so rapidly as to push the curve of hadronic  $\Gamma(M)$  out of agreement with  $\Gamma_{\text{part}}(M)$ .

for sufficiently large  $M$ . We now argue that this possibility does not appear to be realized, at least numerically. Let us smear in  $M$  over a region of size  $\Delta$ ,  $1 \ll \Delta \ll M$ .<sup>6</sup> Owing to the approximate linearity of squared meson masses in the excitation number, there are  $\sim M^3\Delta$  thresholds in this region, and the contribution to the smeared rate from their phase space near the threshold scales as  $M^{-5/2}$  for each.<sup>7</sup> We observe empirically that the magnitudes of amplitudes first appearing at a given threshold mass  $M_{\text{thr}}$  tend to evolve approximately no faster than as  $M_{\text{thr}}^{-0.6}$ . It follows that the contribution to the smeared  $\Gamma(M)$  from the region of width  $\Delta$  scales approximately as  $M^{-0.7}$ . For the border region, where one of the mesons  $m, k$  is highly excited and the other is near the ground state, the phase space is seen to scale as  $M^{-2}$ , but the number of such states is only  $\sim M\Delta$ , so again the area under these peaks contributes little to  $\Gamma(M)$ . Finally, the phase space far above a given threshold scales as  $M^{-3}$ , which means that, given the density of states for various eigenvalue indices, amplitudes cannot on the average grow with  $M$  above their respective thresholds faster than  $M^{1/2}$  for  $k \gg 1$  and  $m \gg 1$ ,  $M^{3/2}$  for one of  $m, k = O(1)$  and the other  $\gg 1$ , or  $M^2$  for  $m$  and  $k = O(1)$ , or else the linear behavior of  $\Gamma(M)$  will be violated. In fact, the amplitudes we have computed all obey these constraints. We see that the linear behavior observed requires a delicate balance of numbers and mass dependences of amplitudes versus excitation numbers, and we hope to obtain analytic arguments for this remarkable behavior in the future.

What are we to conclude from this result? The 't Hooft model is exactly soluble, so it must be the case that the fully-dressed parton diagrams give results agreeing with the hadronic calculation; indeed, this is how the hadronic problem was solved in the first place. The partonic width computed in (4.6) represents only the Born term in an expansion in strong coupling  $g$ , so the addition of gluon loops is apparently necessary to bring the two results into agreement. The small discrepancy between the curves may have this origin, or it may simply be a limitation of the numerical accuracy of the calculation. However, it is interesting to note that the two curves appear to differ asymptotically by a constant, which for plots linear in  $M$  is a  $1/M$  correction. Therefore, we suggest that this effect is genuine and not a numerical artifact. In Fig. 6 we superimpose on the hadronic width of Fig. 4 the curve  $\Gamma_{\text{part}}(M) \cdot (1 + 0.15/M)$ , and see that the fit is outstanding. From this result, we learn that local duality for this system is violated badly only for the first few resonances and very close to thresholds of higher resonances, and that  $1/M$  effects appear to be only at the few percent level for  $M > 7$ . It would be very interesting to see explicitly what happens to the partonic inclusive width at the one- or two-loop level.

---

<sup>6</sup>In practice, we use a normalized Gaussian window function with a mean of  $M$  and a variation of  $\Delta$ , although the result should be independent of the particular form used.

<sup>7</sup>This is verified from (3.1) and the observation that, for  $M \gg 1$ ,  $\mu_0 \propto M$ .

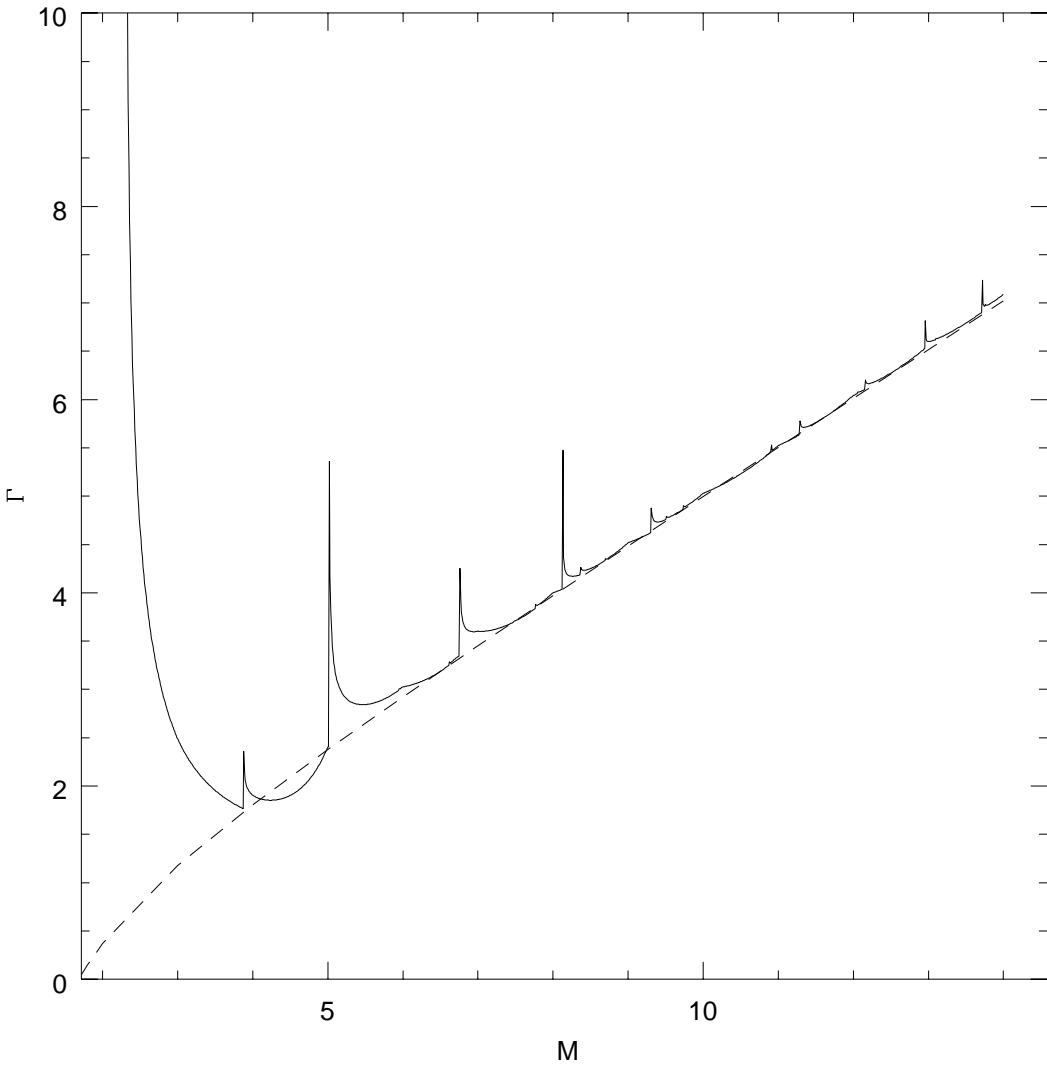


FIG. 6. The full decay width of Fig. 4 compared to the tree-level parton result of Eq. (4.6) corrected by a  $1/M$  effect:  $\Gamma_{\text{part}}(M) \cdot (1 + 0.15/M)$ .

One natural idea of how to improve the Born result is to replace the bare quark masses with the renormalized values. This would not sum all gluon corrections, but it would include an important subclass of them. Unfortunately, due to the result (2.2), masses below 1.0 (such as that of our light antiquark) have *imaginary* renormalized values, and then our whole interpretation of phase space, essential for the calculation of the width, becomes ambiguous.

## VII. CONCLUSIONS

We have calculated the nonleptonic decay width of a heavy-light meson in the context of the 't Hooft model as a function of the bare heavy quark mass, both for the Born term of the free partonic decay (which we called the “partonic width”) and the full sum of allowed

hadronic decays (the “hadronic width”). We found that these two quantities approximately agree at leading order in  $M$ , with the hadronic width being slightly larger. Both quantities are observed to grow linearly and smoothly for large  $M$ , despite the effects of numerous phase space threshold singularities in the hadronic case. The slight discrepancy between hadronic and partonic widths is well-fit by a  $1/M$  correction,  $\Gamma_{\text{hadr}}(M) \approx \Gamma_{\text{part}}(M) \cdot (1 + 0.15/M)$ .

Assuming that the small discrepancy between the partonic and hadronic results is genuine (rather than a numerical artifact) leads one to conclude that nonleptonic heavy-light meson decays in 1+1 dimensions cannot be described in terms of an OPE that lacks  $1/M$  corrections, and it naturally leads one to believe that the same conclusion is true in 3+1. Since the lowest order of the OPE is simply the naive free quark picture, this result also has obvious implications for the application of quark models in such decays. Another incisive test of quark-hadron duality in 1+1 is whether annihilation diagrams, in which the valence quarks in the decaying meson annihilate through a weak current, are suppressed compared to spectator tree diagrams (Fig. 2); these studies are well underway [11], and results will be forthcoming shortly.

A number of unanswered questions not addressed by this work include the effects of loop corrections to the Born amplitude free quark decay, the dependence of decay widths on the light quark mass, the effects of including finite meson strong decay widths (which are  $O(1/N_c)$ ), the effects of identical final state quarks or mesons, multiparticle final states (also suppressed by powers of  $N_c$ ), and so on. While “two-dimensional phenomenology” cannot be used as a quantitative substitute for the standard four-dimensional variety, it clearly indicates the limitations of the standard lore.

*Note Added.* An interesting recent work by Blok [16] suggests that global quark-hadron duality at high energies in the ’t Hooft model with massless quarks may be achieved by including smearing through the  $1/N_c$ -suppressed widths of resonances. Our calculation, on the other hand, does not include finite-width effects but nevertheless achieves an effectively smeared result, even at relatively low  $M$ , which supports the claim of duality at leading order.

### *Acknowledgments*

This work is supported by the Department of Energy under contract DOE-FG03-97ER40506.

## APPENDIX A: THE MULTHOPP TECHNIQUE

This technique [12,15] is used to solve numerically certain singular integral equations in a systematic expansion of basis functions. Specifically, it is used to solve equations of the form

$$\psi(x) = \int_a^b dy K(x, y) \text{Pr} \frac{1}{(x - y)} \cdot \frac{d\psi(y)}{dy}, \quad (\text{A1})$$

where  $\psi(a) = \psi(b) = 0$ . The ’t Hooft equation is seen to be of this form after an integration by parts. Generally speaking, one maps the interval  $y \in [a, b]$  to  $\theta \in [0, \pi]$  by a function linear in  $\cos \theta$ , and then expands in a Fourier series in  $\theta$ . Equivalently, such functions

written directly in terms of  $y$  for each mode turn out to be the product of a common factor  $[\sqrt{y(1-y)}]$  times Chebyshev polynomials of the second kind,  $U_n(y)$ .

In particular, we use a slight variant of the Multhopp technique for the special case that  $K(x, y)$  is independent of  $y$ . The variable transformation is

$$x = \frac{1 + \cos \theta}{2}, \quad y = \frac{1 + \cos \theta'}{2}, \quad (\text{A2})$$

in terms of which the 't Hooft equation may be written

$$\frac{\mu^2}{2} \phi^{M\overline{m}}(\theta) = \frac{(M^2 + m^2) - (M^2 - m^2) \cos \theta}{\sin^2 \theta} \phi^{M\overline{m}}(\theta) + \int_0^\pi d\theta' \frac{d\phi^{M\overline{m}}(\theta')}{d\theta'} \Pr \frac{1}{(\cos \theta - \cos \theta')}. \quad (\text{A3})$$

Expanding

$$\phi^{M\overline{m}}(\theta) = \sum_{m=1}^{\infty} a_m \sin m\theta, \quad (\text{A4})$$

and using the integral ( $m = 0, 1, \dots$ )

$$\int_0^\pi d\theta' \Pr \frac{1}{(\cos \theta' - \cos \theta)} \cos m\theta' = \pi \frac{\sin m\theta}{\sin \theta}, \quad (\text{A5})$$

we are led to a series equation for the eigenvector coefficients  $a_m$ .

We truncate the series after mode  $m = N$ , and evaluate both sides at the equally-spaced values of  $\theta$  (*Multhopp angles*),

$$\theta_k \equiv \frac{k\pi}{N+1}, \quad m = 1 \dots N, \quad (\text{A6})$$

which are a convenient choice because of the inversion identity

$$\sum_{k=1}^N \sin k\theta_m \sin k\theta_n = \frac{1}{2}(N+1)\delta_{mn}, \quad (\text{A7})$$

to obtain at last the finite eigenvector system (compare Ref. [12], Eqs. (A.6)–(A.7))

$$\mu^2 a_n = \frac{4}{(N+1)} \sum_{m=1}^N \sum_{k=1}^N \frac{\sin \theta_{kn} \sin \theta_{km}}{\sin \theta_k} \left\{ \frac{(M^2 + m^2) - (M^2 - m^2) \cos \theta_k}{\sin \theta_k} + m\pi \right\} a_m. \quad (\text{A8})$$

The series expansion (A4) transforms the normalization condition  $\int_0^1 dx \phi(x)^2 = 1$  into

$$1 = - \sum_{m=1}^N m a_m \sum_{n=1}^N n a_n \left[ 1 + (-1)^{m+n} \right] \left[ (1 - (m-n)^2) (1 - (m+n)^2) \right]^{-1}, \quad (\text{A9})$$

while the phase of the eigenvectors may be chosen by noting the asymptotic forms

$$\phi(x) \rightarrow -2\sqrt{x} \sum_{m=1}^N (-1)^m m a_m + O(x), \quad (\text{A10})$$

as  $x \rightarrow 0$ , and

$$\phi(x) \rightarrow +2\sqrt{1-x} \sum_{m=1}^N m a_m + O(1-x), \quad (\text{A11})$$

as  $x \rightarrow 1$ . Note that the Multhopp solution requires the eigenfunctions to vanish as square roots at the endpoints, in contrast to the dynamically-generated exponents of the exact solution given by Eq. (2.5). Great care must be exercised when extracting information near the endpoints of the numerically-calculated wave functions.

In terms of the eigenvector components  $a_m$ , the vertex function  $\Phi$  may be written for real  $x$ ,

$$\Phi(x < 0) = \frac{-\pi}{\sqrt{x(x-1)}} \sum_{m=1}^N (-1)^m m a_m \left( \sqrt{1-x} - \sqrt{-x} \right)^{2m}, \quad (\text{A12})$$

and

$$\Phi(x > 1) = \frac{+\pi}{\sqrt{x(x-1)}} \sum_{m=1}^N m a_m \left( \sqrt{+x} - \sqrt{x-1} \right)^{2m}. \quad (\text{A13})$$

These regions are the only ones for which we need explicit expressions; whenever  $x \in (0, 1)$ , the 't Hooft equation (2.4) and the definition (2.6) may be employed to rewrite  $\Phi(x)$  in terms of  $\phi(x)$ .

Because of the singularities in  $\Phi$  at  $x = 0$  and  $1$ , when numerically computing overlap integrals such as in Eqs. (5.7), (5.10), or (5.11), one must sample the region near the singularities more heavily. Moreover, in contrast to the numerical Multhopp solution for  $\Phi(x)$  given above, the singularities in the exact solution behave as  $\Phi^{M\bar{m}}(x \rightarrow 0^-) \sim (-x)^{\beta_M-1}$  and  $\Phi^{M\bar{m}}(x \rightarrow 1^+) \sim (1-x)^{\beta_m-1}$ . Such a difference can also lead to substantial errors when computing overlap integrals; the answer is to increase the number of eigenvector modes in the wave function solution, so as to decrease the size of the region where the asymptotic behaviors differ.

Finally, the quantity  $c_n$ , which is the meson decay constant up to a normalization factor (Eq. (2.7)), is simply given by

$$c_n \equiv \int_0^1 dx \phi_n(x) = \frac{\pi}{4} a_1. \quad (\text{A14})$$

## APPENDIX B: AMPLITUDE SUM RULES

The asymptotic forms of 't Hooft model solutions may be used to obtain constraints on the form factor expressions, such as Eqs. (5.3)–(5.4), that are derived from them, as is shown in [9]. There it is seen that, as  $|q^2| \rightarrow \infty$ , the form factors vanish at least as fast as  $|q^2|^{1+\beta_m}$ , where  $\beta_m$  is defined in Eq. (2.5). By symmetry there is also a term that falls off as  $|q^2|^{1+\beta_M}$ , but since  $M > m$ , we have  $\beta_M > \beta_m$ , and the slower fall-off dominates.

It is then apparent from Eqs. (5.3)–(5.4) that the pole residue functions  $\mathcal{A}_n(q^2)$  and  $\mathcal{B}_n(q^2)/q^2$  must also vanish at least as fast as  $|q^2|^{\beta_m}$ . But (5.3) and (5.4) have a very

suggestive form: They explicitly display the pole-dominance nature of the large- $N_c$  limit, since  $\mathcal{A}_n(q^2)$  and  $\mathcal{B}_n(q^2)/q^2$  are expected to have no non-analytic behavior for finite  $q^2$ , and moreover, these expressions are written very conveniently for an application of Cauchy's theorem. If we choose our contour such that it encloses all of the complex  $q^2$  plane except for the part of the real axis where the resonance poles lie, then using Cauchy's theorem with the vanishing of the residue functions for  $|q^2| \rightarrow \infty$  gives [9]

$$\sum_n \frac{\Lambda_n(q^2)}{1 - q^2/\mu_n^2} = \sum_n \frac{\Lambda_n(\mu_n^2)}{1 - q^2/\mu_n^2}, \quad (\text{B1})$$

where  $\Lambda_n(q^2) = \mathcal{A}_n(q^2)$  or  $\mathcal{B}_n(q^2)/q^2$ , and the sums over  $n$  are restricted to the appropriate parities. Each residue function thus needs only to be computed at the value of its corresponding mass eigenvalue.

This sum rule also gives us enough information, in principle, to obtain residue functions that are not conveniently computable in a direct fashion [12]. Let  $t$  denote some threshold in  $n$ , below which it is unwieldy to compute the residue functions directly. Then, if we choose at least  $t$  values of  $q_i^2$ ,  $i = 1 \dots t$  above threshold, we obtain a solvable  $t \times t$  linear system of equations:

$$\sum_{n \leq t} \frac{\Lambda_n(\mu_n^2)}{1 - q_i^2/\mu_n^2} = - \sum_{n > t} \frac{\Lambda_n(\mu_n^2)}{1 - q_i^2/\mu_n^2} + \sum_n \frac{\Lambda_n(q_i^2)}{1 - q_i^2/\mu_n^2}. \quad (\text{B2})$$

Adding additional  $q_i^2$  simply overconstraints the system and provides consistency checks. We refer to this approach in the text as “backsolving”, to indicate that it is an indirect method of solution.

We also note one other sum rule [9,12], which is simply derived by taking the limit  $q^2 \rightarrow \infty$  in (B1) and recalling that the form factor expressions vanish in this limit:

$$\sum_n \mu_n^2 \Lambda_n(\mu_n^2) = 0. \quad (\text{B3})$$

## REFERENCES

- [1] E. D. Bloom and F. J. Gilman, Phys. Rev. Lett. **25**, 1140 (1970).
- [2] J. D. Richman, in Proceedings of *The 28th International Conference on High-Energy Physics (ICHEP96)*, Edited by Z. Ajduk and A. K. Wroblewski (World Scientific, Singapore, 1997), p. 143.
- [3] I. Bigi, B. Blok, M. A. Shifman, and A. Vainshtein, Phys. Lett. **B323**, 408 (1994).
- [4] E. Bagan, P. Ball, V. M. Braun, and P. Gosdzinsky, Phys. Lett. **B342**, 362 (1995); *ibid.*, **B374**, 363(E) (1996).
- [5] I. I. Bigi, B. Blok, M. Shifman, N. G. Uraltsev, and A. Vainshtein, in Proceedings of *The Fermilab Meeting: DPF 92*, Edited by Carl H. Albright, Peter H. Kasper, Rajendran Raja, and John Yoh. (World Scientific, River Edge, N.J., 1993), p. 610.
- [6] G. 't Hooft, Nucl. Phys. B **75**, 461 (1974).
- [7] G. 't Hooft, Nucl. Phys. B **72**, 461 (1974);  
E. Witten, Nucl. Phys. B **160**, 57 (1979) provides an excellent review of these properties.
- [8] C. G. Callan, Jr., N. Coote, and D. J. Gross, Phys. Rev. D **13**, 1649 (1976).
- [9] M. B. Einhorn, Phys. Rev. D **14**, 3451 (1976).
- [10] G. Altarelli, G. Martinelli, S. Petrarca, and F. Rapuano, Phys. Lett. **B382**, 409 (1996).
- [11] B. Grinstein and R. F. Lebed, in preparation.
- [12] R. L. Jaffe and P. F. Mende, Nucl. Phys. B **369**, 189 (1992).
- [13] B. Grinstein and P. F. Mende, Phys. Rev. Lett. **69**, 1018 (1992).
- [14] B. Grinstein and P. F. Mende, Nucl. Phys. B **425**, 451 (1994).
- [15] A. J. Hanson, R. D. Peccei, and M. K. Prasad, Nucl. Phys. B **121**, 477 (1977);  
K. Karamcheti, *Principles of Ideal-Fluid Aerodynamics* (John Wiley & Sons, New York, 1966).
- [16] B. Blok, University of Minnesota preprint UMN-TH-1452-9 [hep-ph/9707218] (unpublished).

## Figure Captions

FIG. 1. Parton decay diagram for the inclusive decay. Of interest are the parton labels, as used in the text.

FIG. 2. Diagram for “tree” (T) meson exclusive decay. Numbers indicate quark labels used in the text (except **0**, which refers to the ground-state “ $\bar{B}$ ” meson), while letters indicate the eigenvalue index of meson resonances. One can also consider contact-type diagrams, in which the point labeled by **n** is not coupled to a resonance.

FIG. 3. Weak decay amplitude  $\mathcal{M}_T$  for the exclusive decay to the lowest mode  $\mathbf{0} \rightarrow (\mathbf{m} = 0), (\mathbf{k} = 0)$ , as a function of heavy quark mass  $M$ , with light quark mass  $m = 0.56$ . The overall factor  $2\sqrt{2/\pi} G_F V_{31} V_{45}^* (c_V^2 - c_A^2)$  in the amplitude is suppressed for convenience.

FIG. 4. The full decay width for the sum of exclusive modes in the decay  $\mathbf{0} \rightarrow \mathbf{mk}$  as a function of heavy quark mass  $M$ , with light quark mass  $m = 0.56$ . The overall factor  $8G_F^2 |V_{31} V_{45}^*|^2 (c_V^2 - c_A^2)^2 / \pi$  in the width is suppressed for convenience. The dashed line is the tree-level parton result, Eq. (4.6).

FIG. 5a. The full decay width as a function of heavy quark mass  $M$ , with light quark mass  $m = 0.56$ , including only the exclusive mode with the lowest threshold value (corresponding to  $\mathbf{m} = \mathbf{k} = 0$ ). The scale is the same as in Fig. 4.

FIG. 5b. Same as Fig. 5a, except now including the exclusive modes corresponding to the *three* lowest threshold values.

FIG. 5c. Same as Fig. 5a, except now including the exclusive modes corresponding to the *five* lowest threshold values.

FIG. 5d. Same as Fig. 5a, except now including the exclusive modes corresponding to the *eleven* lowest threshold values. Observe that this figure is almost indistinguishable from the full result, Fig. 4.

FIG. 6. The full decay width of Fig. 4 compared to the tree-level parton result of Eq. (4.6) corrected by a  $1/M$  effect:  $\Gamma_{\text{part}}(M) \cdot (1 + 0.15/M)$ .